Broadband Wavelength Conversion for Hybrid Multiplexing Signals Based on a Parallel Dispersion-Engineered Silicon Waveguide

Baobao Chen, Yi Zhao, Haoyang Tan, Xiaowei Guan, and Shiming Gao, *Member, IEEE*

***Abstract*—Broadband all-optical wavelength conversion (AOWC) for hybrid wavelength- and mode-division multiplexing (WDM-MDM) signals is experimentally demonstrated based on degenerate four-wave mixing in a silicon chip with a parallel dispersion-optimized multimode nonlinear waveguide and mode (de)multiplexers. By simultaneously coupling two modes into the waveguide using an optical fiber array, the intermodal crosstalk is measured to be as low as −25.9 dB for the fundamental mode of the transverse electric mode (TE_0) (or −23.6 dB for the first-order mode TE_1), and the conversion efficiency is −25.4 dB for TE_0 (or −26.3 dB for TE_1) mode. A wide conversion bandwidth of ∼68 nm is measured except for the influence of the crosstalk, which is the first time to experimentally demonstrate the broadband wavelength conversion for MDM signal. Using a 4 × 10 Gbit/s on-off keying (OOK) hybrid WDM-MDM signal, four AOWC channels are obtained on the idlers and the power penalty of each channel is less than 2.7 dB at the bit-error-ratio of 1×10^{-9}.**

***Index Terms*—Hybrid multiplexing signals, broadband wavelength conversion, multimode nonlinear waveguide, intermodal crosstalk.**

I. Introduction

MULTIPLEXING technologies have been paid much more attention as the demand of the link capacity increases rapidly, which can transfer multi-channel data in parallel by effectively utilizing multiple wavelengths, multiple modes, as well as dual polarization. Nowadays, single multiplexing technologies including wavelength-division multiplexing (WDM) [1], [2], mode-division multiplexing (MDM) [3], [4], or polarization-division multiplexing (PDM) [5] have been well investigated. However, these multiplexing technologies employ only mono dimensional physical property of optical carriers. In order to effectively enhance the transmission capacity, hybrid multiplexing technologies by compatibly combining several multiplexing technologies together and extending more physical properties of one optical carrier are considered, such as the combination of PDM-MDM [6], [7], WDM-MDM [8], [9], [10], or WDM-PDM signals [11], [12]. As an additional degree of freedom, WDM-PDM technology can enable two polarization signals to be carried on one wavelength channel, which doubles the transmission capacity relative to WDM technology. In particular, hybrid WDM-MDM technology can multiply the transmission capacity by utilizing each wavelength channel carrying multiple modes. Many investigations have focused on hybrid WDM-MDM technology. For example, the elliptical-core highly nonlinear few-mode fiber (FMF) based optical cross-connect scheme has been proposed in WDM-MDM networks [13]. The long distance WDM-MDM transmission in FMF by using all fiber mode multiplexers has been demonstrated [14]. Moreover, the WDM-MDM signal transmission has also been proposed in silicon photonic integrated circuits. For example, a 32-channel hybrid WDM-MDM de-multiplexer based on silicon has been designed with an intermode crosstalk of −16.5 to −23.5 dB [15].

On-chip optical signal processing is essential for future all-optical communication networks. Multidimensional multiplexing all-optical wavelength conversion (AOWC) technology is considered to be one of the key technologies for future optical transport networks, which is important for enhancing the network reconfigurability and non-blocking capability. For MDM signals, most of the researches are still limited to the AOWC for the single-mode signal or mode-selective signal due to the complexity of modes in optical fibers and waveguides [16], [17], [18], [19]. A mode-selective on-chip AOWC is realized based on FWM with a wavelength conversion efficiency of −33 dB, and the conversion bandwidth is only 1.2 nm [16]. A conversion bandwidth of 10 nm is obtained in a cross-phase modulation (XPM)-based AOWC [18]. In order to support more WDM channels, a high conversion bandwidth is urgent to a AOWC device. In our previous contributions, the theoretical models of broadband AOWC have been proposed for MDM signals in dual-mode fibers and multimode silicon waveguides [20], [21], [22]. To support a broadband conversion of the MDM signal, the dispersion profiles of the nonlinear waveguide have to have very small discrepancy between different modes in the wide

Manuscript received 19 October 2022; revised 9 December 2022; accepted 19 December 2022. Date of publication 26 December 2022; date of current version 30 December 2022. This work was supported in part by the National Key Research and Development Program of China under Grant 2019YFB2205202, in part by the Zhejiang Provincial Natural Science Foundation of China under Grant LD19F050001, and in part by the National Natural Science Foundation of China under Grants 61875172 and U2141231. *(Corresponding author: Shiming Gao.)*

Baobao Chen, Yi Zhao, Haoyang Tan, and Shiming Gao are with the Centre for Optical and Electromagnetic Research, State Key Laboratory of Modern Optical Instrumentation, International Research Center for Advanced Photonics, Zhejiang University, Hangzhou 310058, China, and also with the Ningbo Research Institute, Zhejiang University, Ningbo 315100, China (e-mail: chenbaobao@zju.edu.cn; 11930056@zju.edu.cn; dgxythy@zju.edu.cn; gaosm@zju.edu.cn).

Xiaowei Guan is with the Intelligent Optics & Photonics Research Center, Jiaxing Institute of Zhejiang University, Jiaxing 314031, China, and also with the DTU Fotonik, Department of Photonics Engineering, Technical University of Denmark, 2800 Lyngby, Denmark (e-mail: guanxw@zju.edu.cn).

Digital Object Identifier 10.1109/JPHOT.2022.3231345

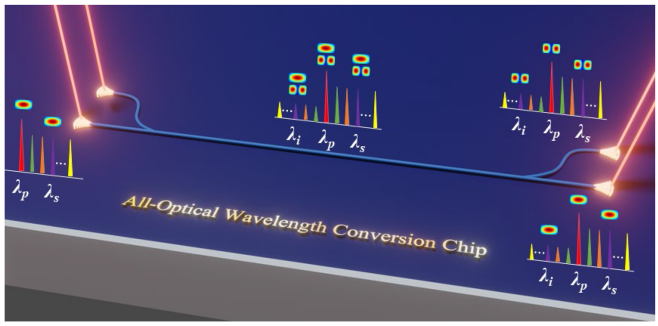

Fig. 1. Schematic diagram of the on-chip FWM-based AOWC for the WDM-MDM signal.

conversion band, which is a big challenge for the waveguide design and fabrication. In addition, multiple tributaries need to be simultaneously coupled with high efficiency in experiments and the adjustment difficulty also increases. For the hybrid multiplexing signal, the AOWC has been achieved in a highly nonlinear fiber for the 8-WDM-PDM 32 Gbaud 16-QAM signals [23]. So far, the broadband AOWC for hybrid multiplexing signals based on silicon waveguides has not yet been reported.

In this paper, we experimentally demonstrate the FWM-based broadband AOWC scheme for hybrid WDM-MDM signals in a fabricated AOWC chip, which consists of a parallel dispersion-engineering multimode nonlinear silicon waveguide and a pair of MUX and de-MUX. A dual-channel optical fiber array (OFA) is utilized to achieve simultaneous coupling of the signals. The fabricated chip features a wide conversion bandwidth of 68 nm, a low intermodal crosstalk of -25.9 dB for TE_0 mode or -23.6 dB for TE_1 mode, and a high wavelength conversion efficiency of -25.4 dB for TE_0 mode or -26.3 dB for TE_1 mode, respectively. Testing by a four-channel 10 Gbit/s on-off keying (OOK) WDM-MDM signal, the converted power penalty of each channel is less than 2.7 dB at the BER of 1×10^{-9}. The demonstrated AOWC scheme for WDM-MDM signals is promising for high-speed data transmission systems.

II. Principle

Fig. 1 shows the schematic diagram of the on-chip AOWC for hybrid WDM-MDM signals. Multiple-wavelength TE_0 signals (λ_{S1}, λ_{S2}, λ_{S3}, …, λ_{Sn}) are separated to two branches and coupled into the chip via two focused shallow etched grating couplers. And then, one branch is converted to TE_1 mode through a mode multiplexer to form the WDM-MDM signal. If a high-power TE_0 pump (λ_P) is injected into the chip together with the signal, a dual-mode pump can be obtained in the dispersion-engineered multimode nonlinear waveguide, where multiple FWM processes will occur, including six different types among the dual-mode pump and the MDM signal on a single wavelength [21]. However, only four processes among them are efficient due to their small phase mismatches: FWM1 ($2P^{TE0} \rightarrow S^{TE0}+C^{TE0}$) and FWM2 ($2P^{TE1} \rightarrow S^{TE1}+C^{TE1}$) are the desired intra-modal processes for AOWC, while FWM3 ($P^{TE0}+P^{TE1} \rightarrow S^{TE1}+C^{TE0}$) and FWM4 ($P^{TE0}+P^{TE1} \rightarrow S^{TE0}+C^{TE1}$) are the intermodal FWM processes that serve as crosstalk [24]. Multiple-wavelength converted idlers ($\lambda_{C1}, \lambda_{C2}, \lambda_{C3}, \ldots, \lambda_{Cn}$) with dual modes that carry the same data as the signal on each wavelength will be generated. Therefore, the WDM-MDM signal is all-optical converted to the idler wavelengths. The converted WDM-MDM signal on the idlers are separated in mode by a mode de-multiplexer and output from the chip. The TE_0 modes of all the wavelength channels are output from CH1 port, while the TE1 modes are output from CH2 port. Each wavelength can be further filtered for detection.

III. Chip Fabrication and Characterization

The dispersion-engineered silicon waveguide is designed by fixing the thickness of silicon at 220 nm and tuning the width to optimize the dispersion curves of the TE_0 and TE_1 modes. In order to support FWM1 and FWM2 simultaneously over a wide bandwidth, the phase-matching conditions need to be satisfied, with the phase mismatch close to zero over a large wavelength range. It means that the dispersion curves of the two modes should be flat and nearly identical. Also, the zero-dispersion wavelengths (ZDWs) of the two modes should be near 1550 nm. Therefore, several geometrical parameters of the waveguide structure are optimized. On the basis of the precise adjustment of the waveguide cross-section dimensions according to the dispersion of different modes, the waveguide length as a new geometry parameter is added to position the waveguide size more accurately for phase matching of the parallel FWM processes in a wideband. In this way, the waveguide width is optimized as 770 nm. The mode (de)multiplexer (MUXs/de-MUXs) is realized by utilizing the adiabatic tapered couplers (ATCs), which consists of two adiabatic tapered waveguides: the narrow waveguide has a tapering width that changes from 260 nm to 150 nm, and the wide waveguide has a width from 480 nm to 770 nm. The coupling length is 15 μm and the coupling gap is 200 nm [22]. The mode multiplexers are designed based on ATCs, which exhibit good tolerance in waveguide width and enable efficient coupling with large bandwidth [24].

The optimized chip structure is fabricated on a SOI wafer with 220-nm silicon on top of a 3-μm buried-oxide (BOX) layer. Two steps of electron-beam lithography (EBL) and inductive plasma-etching (ICP) were used to first define the fully etched waveguides and then the shallowly (70 nm) etched grating couplers. The electron-sensitive resists used in both the two steps were CSAR (AR-P 6200.09) and the etchants were the gas mixture of sulfur hexafluride (SF6, 38 sccm) and octafluorocyclobutane (C4F8, 70 sccm). The fabricated sample was finally covered with a 1-μm SiO_2 layer using a plasma-enhanced chemical vapor deposition (PECVD) machine.

Fig. 2(a) shows the scanning electron microscope (SEM) photos of the fabricated chip. The focused shallow etched grating coupler is zoomed in Fig. 2(b), which is suitable for TE_0 mode and used as the input and output port of the chip. Fig. 2(c) details the microscope image of the MUX, and the structure of the de-MUX is the same as that of the MUX. Fig. 2(d) shows the straight multimode nonlinear waveguide, which has high width uniformity and surface smoothness.

The total insertion loss and mode crosstalk are measured by testing the transmission of the back-to-back MUX and de-MUX structures with the input from the MUX CH1 or CH2 port, as

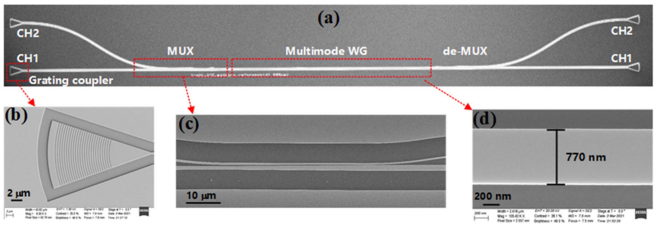

Fig. 2. SEM photos of (a) the fabricated silicon chip for multimode device, (b) a focusing shallow etched grating coupler, (c) TE_0 and TE_1 mode multiplexer details, and (d) dispersion-engineered multimode nonlinear waveguide.

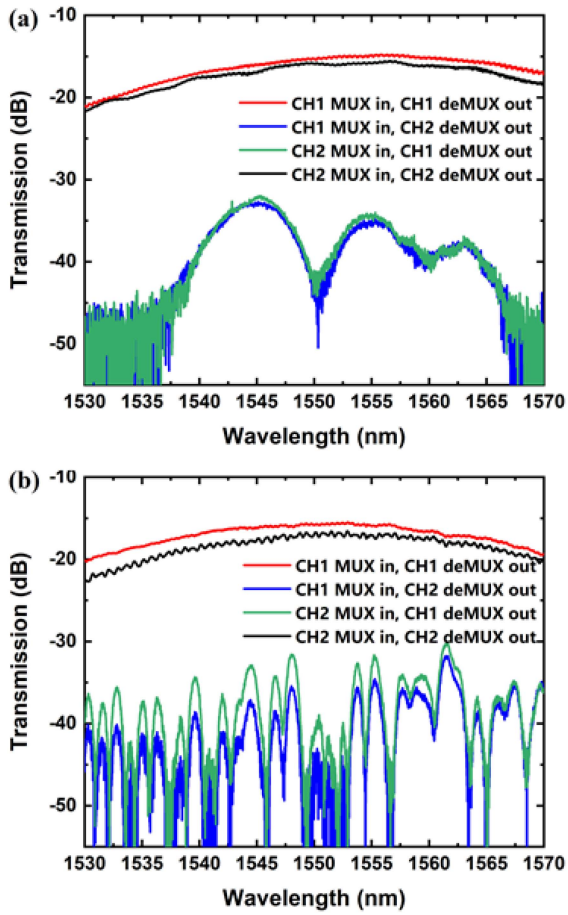

Fig. 3. Measured transmission spectrums of (a) the back-back MUX and de-MUX structure and (b) the AOWC structure.

shown in Fig. 3(a). Here, the transmission is normalized by the incident light power, which is measured to be 10 mW. In principle, the incident light from the MUX CH2 port will be received at the de-MUX CH2 port through twice mode conversions. While, the light from the MUX CH1 will be preserved as the TE_0 mode and output from the de-MUX CH1 port. The light output from the other port is considered as the crosstalk. In Fig. 3(a), the total insertion losses are calculated to be around 15.3 dB and 15.8 dB for CH1 port and CH2 port, respectively, which are attributed to the major coupling losses of 7.4 dB/facet. The mode crosstalk is around −26.9 dB for TE_0 and −26.4 dB for TE_1 at 1550 nm, respectively. Fig. 3(b) shows the transmission of the AOWC structure with a 2.9-mm-long multimode nonlinear waveguide

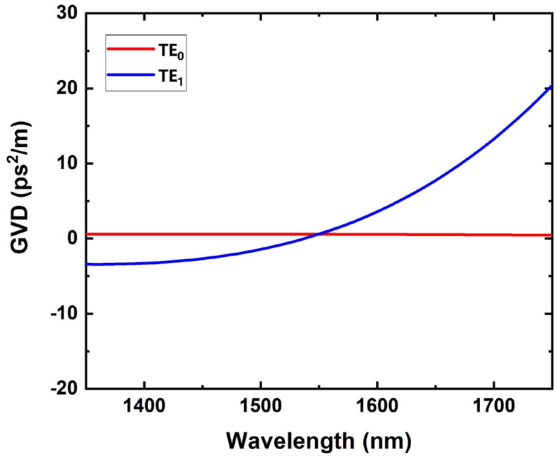

Fig. 4. GVD profiles of the TE_0 and TE_1 modes when the waveguide height is 220 nm and the waveguide width is 770 nm.

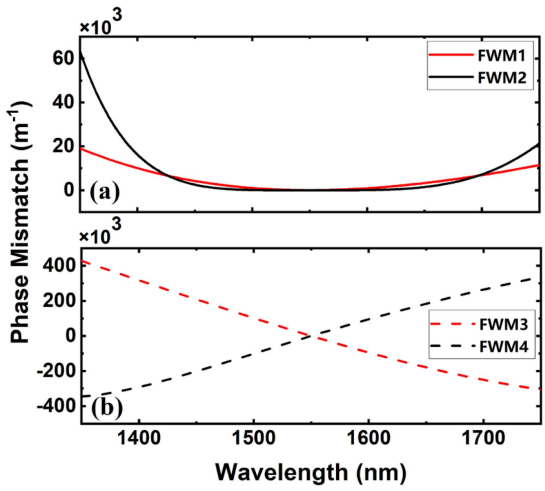

Fig. 5. Simulated phase mismatch profiles of the four FWM processes.

between the MUX and de-MUX. The crosstalk is −26.6 dB for TE_0 and −26.2 dB for TE_1 at 1550 nm, which is almost the same as that in Fig. 3(a) without the nonlinear waveguide. By comparing the transmission spectrum in Fig. 3(a) and (b), the propagation losses of the nonlinear waveguide can be calculated, which are about 1.2 dB/cm for TE_0 and 3.0 dB/cm for TE_1. In addition, the transmission of the chip shows the broadband performance, which is wide enough to cover the wavelength range from 1500 to 1600 nm [22].

According to the fabricated dimensions, the group-velocity dispersion (GVD) profiles of the nonlinear waveguide are simulated for the TE_0 and TE_1 modes, as shown in Fig. 4. The GVD curve of the TE_0 mode is close to zero over C-band and it is around 0.61 ps^2/m and the ZDW of the TE_1 mode is 1555.5 nm. In the wavelength range of 1515∼1585 nm, the GVD discrepancy between the two modes is no more than 1.1 ps^2/m, which is promising to support the broadband AOWC for WDM-MDM signals. In addition, the phase mismatch profiles of the four FWM processes versus the signal wavelength are simulated, as shown in Fig. 5 [22]. Fig. 5(a) shows the phase mismatch curves

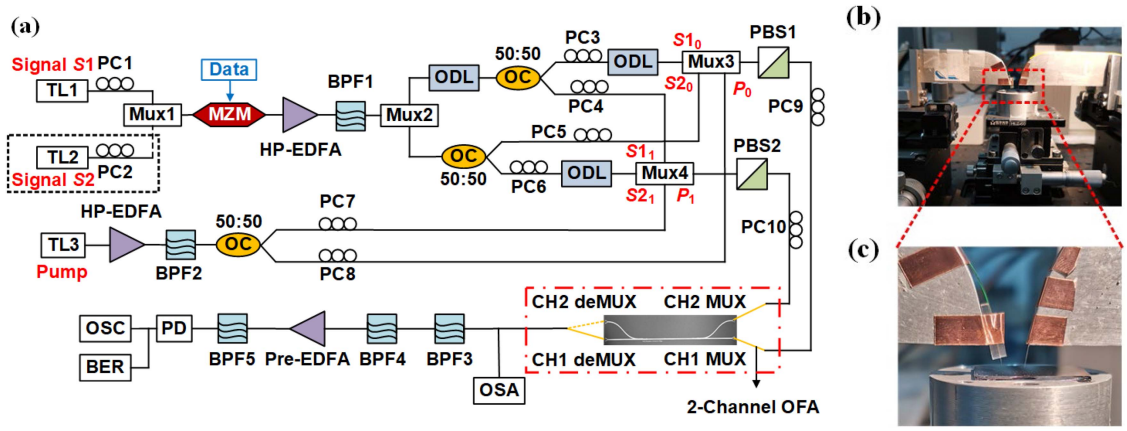

Fig. 6. (a) Experimental setup of the AOWC scheme for the WDM-MDM hybrid multiplexing signals; (b) the fiber-to-chip coupling platform; (c) the two-channel optical fiber array.

of FWM1 and FWM2, which are flat and close to zero. When the signal is near the pump, the phase mismatches of FWM3 and FWM4 will be also close to zero, as shown in Fig. 5(b). In this case, FWM3 and FWM4 occur sufficiently to introduce heavy crosstalk to FWM1 and FWM2 that we need. Fortunately, the phase mismatches of FWM3 and FWM4 increase rapidly, and the crosstalk is efficiently suppressed as the signal moves away from the pump. Therefore, it is expected to support the broadband AOWC for WDM-MDM signals.

IV. Broadband AOWC for MDM Signal

Fig. 6(a) shows the experimental setup for the proposed AOWC scheme for WDM-MDM signals in the dispersion-engineered silicon waveguide. Two CW optical carriers are provided by a multichannel tunable laser with a linewidth of 100 kHz (Agilent N7714A) and combined together via a multiplexer (MUX1). The OOK signals $S1$ and $S2$ with different wavelengths λ_1 and λ_2 are generated by modulating a 2^{31}-1 NRZ pseudo-random bit sequence (PRBS) pattern on the signal carriers via a Mach-Zehnder modulator. After amplified by a high-power erbium-doped fiber amplifier (HP-EDFA), the signals $S1$ and $S2$ are separated by MUX2 and each of them are split into two tributaries of $S1_0$ and $S1_1$ (or $S2_0$ and $S2_1$) via a 3-dB optical coupler (OC) so as to excite the TE_0 and TE_1 modes. The optical delay lines (ODLs) are introduced to eliminate the correlation of different channels. A CW pump P provided by a tunable laser (YOKOGAWA AQ2200) is amplified by a HP-EDFA. After being split into two tributaries of P_0 and P_1 by a 3-dB coupler, the pump is combined with the signals via multiplexers (MUX3 and MUX4), which have a 0.8-nm-wide bandwidth to suppress the EDFA noises. PCs (PC3∼PC8) and PBSs are employed to adjust the polarization states of the pump and signals to ensure their co-polarization. Their polarization states are aligned to the axes of the silicon waveguide by adjusting PC9 and PC10. The fiber-to-chip coupling platform supports the three-dimensional precision adjustment, as shown in Fig. 6(b). To simultaneously achieve fiber-to-chip coupling for two tributaries, a two-channel OFA with a 127-μm pitch is used, as shown in Fig. 6(c). The position and angle of the OFA is carefully adjusted to ensure that both of the two-tributary coupling powers reach their maximums. In the multimode nonlinear waveguide, the TE_0 and the excited TE_1 modes from the signals ($S1_0$, $S1_1$, $S2_0$, $S2_1$) and pumps (P_0, P_1) interact through FWM processes to generate four-channel converted signals on the TE_0 and TE_1 modes of the generated idlers with two different wavelengths. The output spectrum is measured by an optical spectrum analyzer (OSA, Ando AQ6317B). The TE_0 mode channel and the TE_1 mode channel are separated by the de-MUX structure and output at the CH2 port and CH1 port respectively. Also, the idlers are filtered by the band-pass filters (BPF3 and BPF4) with a 0.8-nm-wide bandwidth, pre-amplified by pre-EDFA, and observed using an optical oscilloscope (Agilent Infiniium 86100A). The BPF1, BPF2 and BPF5 are used to filter out the ASE noise introduced by the EDFA.

The broadband AOWC of the single MDM signal is demonstrated by simultaneously injecting signal $S1$ and pump P. The signal $S1$ is provided by one channel of the tunable laser (Agilent N7714A). Their wavelengths are set at 1547.7 nm and 1550.1 nm, and the corresponding powers of their tributaries before the MUX of the chip are around 20.2 dBm and 23.5 dBm, respectively. The idler is generated at 1552.5 nm, whose TE_0 and TE_1 modes from FWM1 and FWM2 carrying the same OOK sequences as the signal. Using a 5 Gbit/s OOK MDM signal, the bit-error-ratio (BER) is measured as a function of the received power, as shown in Fig. 7(a), where the back-to-back (B2B) case is also measured for comparison. Here, the crosstalk from FWM3 and FWM4 is evaluated by injecting the two modes separately or together. When the TE_0 mode is input, the power penalty (at BER of 10^{-9}) of the TE_0 mode idler generated from FWM1 is 1.7 dB in comparison to the B2B signal, while it is 1.9 dB for the TE_1 mode idler. By injecting the pump and the signal at the two ports of the chip simultaneously, the crosstalk from FWM3 and FWM4 will be introduced, companying the generation of the required AOWC MDM signal. As a result, the power penalty is further degraded by 0.5 dB or 0.6 dB for the TE_0 or TE_1 mode. The clear eye-diagrams of the MDM signal on the idlers are observed, as illustrated in the inset of

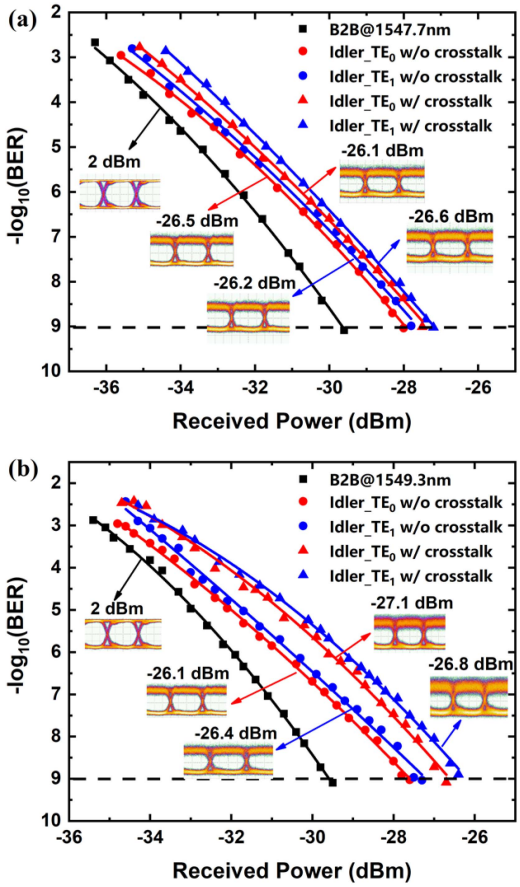

Fig. 7. BER for the converted TE_0 and TE_1 modes on the idler with the signal wavelength of (a) 1547.7 nm or (b) 1549.3 nm.

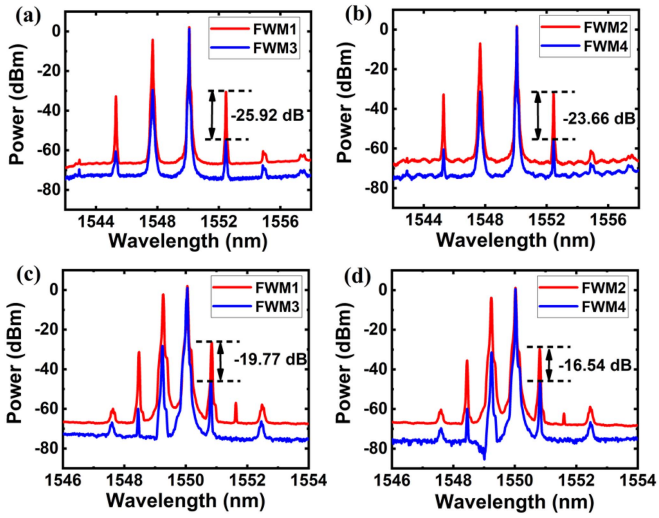

Fig. 8. Measured output spectrums at the output port of (a) CH1 or (b) CH2 for the signal channel at 1547.7 nm, and the measured output spectrums at the output port of (c) CH1 or (d) CH2 for the signal channel at 1549.3 nm.

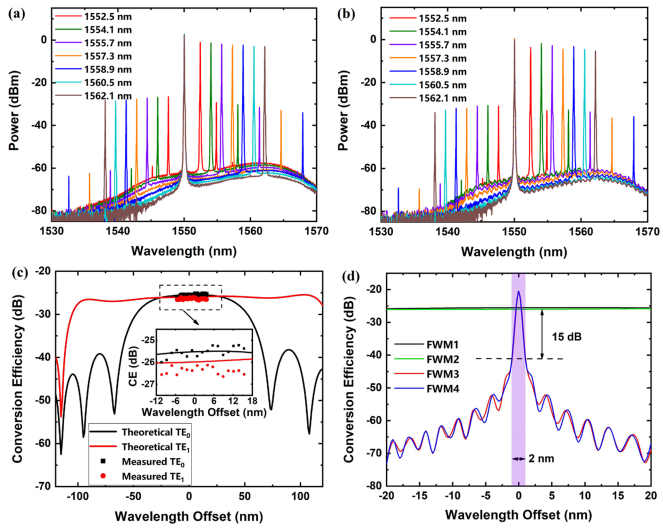

Fig. 9. Spectra measured of wavelength conversion for (a) TE0 and (b) TE1 mode signals at different channels from 1552.5 nm to 1562.1 nm, (c) the conversion bandwidths for TE_0 and TE_1 modes, and (d) the simulated conversion efficiencies for the four FWM processes.

Fig. 7(a). In order to evaluate the conversion performance in different channels, the signal wavelength is adjusted closer to the pump and set at 1549.3 nm. The corresponding results are shown in Fig. 7(b). The extra power penalties increase to 1.0 dB and 0.9 dB. The reason lies in that the AOWC for the signal near the pump is more affected by the crosstalk from the FWM processes that are not expected.

In order to quantitatively analyze the crosstalk effects, the FWM spectrums at the two output ports of the chip are measured, as shown in Fig. 8, where the resolution of the OSA is 0.05 nm and the absolute accuracy is 0.3 dB. For the signal channels at 1547.7 nm and 1549.3 nm, Fig. 8(a) and (c) show the output spectrums at CH1 output port by injecting the pump from the two input ports and the signal from CH1 or CH2 input port, respectively. In this case, the TE_0 idlers from FWM1 and FWM3 can be obtained separately, as shown in the red and blue curves. An extra crosstalk of 6.2 dB is introduced when the signal moves from 1547.7 nm to 1549.3 nm. Fig. 8(b) and (d) depict the spectrums at CH2 output, where the red and blue curves represent the TE_1 idlers from FWM2 and FWM4, respectively. The crosstalk increases by 6.9 dB for TE_1 mode. The crosstalk observed in Fig. 8 can be explained according to the phase mismatch profiles in Fig. 5.

The conversion bandwidth is evaluated by fixing the pump P at 1550.17 nm and the signal $S1$ is tuned from 1552.5 nm to 1562.1 nm (1.6 nm step), as shown in Fig. 9(a) and (b), which correspond to the TE_0 and TE_1 modes, respectively. The converted idlers with a wavelength of 1538.09 nm to 1547.63 nm can be clearly observed. Some other idlers that are not required can also be generated in the waveguide via some other FWM processes including $2S^{TE0} \rightarrow P^{TE0} + C^{TE0}$ and $2S^{TE1} \rightarrow P^{TE1} + C^{TE1}$. According to the spectrums in Fig. 9(a) and (b), the conversion efficiency can be obtained, which are shown in the inset of Fig. 9(c). Since the measured wavelength range is limited by the tunable ability of the laser, the entire response curves are fitted for both the TE_0 and TE_1 modes, as shown in Fig. 9(c). The experiments are in excellent agreement with simulations, showing the potential of the device for broadband conversion. From the response curves of the conversion efficiency, the conversion

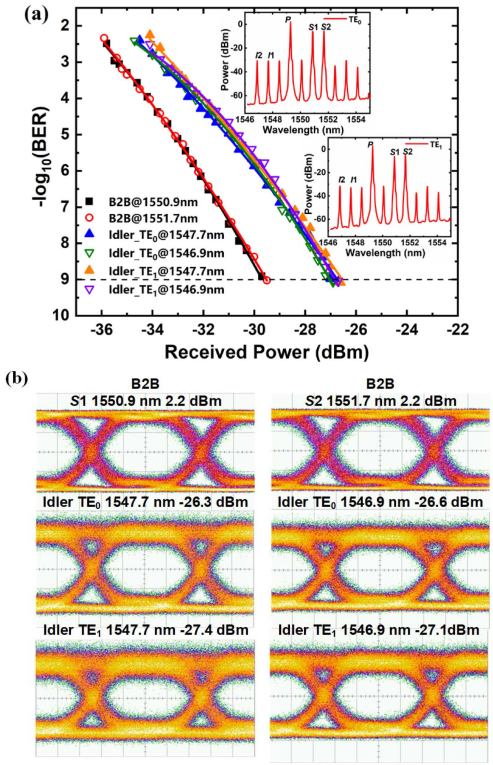

Fig. 10. (a) Measured BERs against the received power for the WDM-MDM signals (B2B) and the idlers; (b) eye diagrams of the WDM-MDM signals and the converted idlers.

bandwidth can be read, which are both about 70 nm. According to our previous study [20], [21], [22], the performance of the FWM1 and FWM2 is affected by the FWM3 and FWM4 when the signal is near the pump. The conversion efficiencies of four FWM processes are simulated in Fig. 9(d). One can find that the crosstalk is too heavy to ensure the signal quality within a 2 nm wavelength range around the pump, which should be excepted from the band width. As a result, the conversion bandwidths are both about 68 nm for TE_0 and TE_1 modes.

V. Realization of the AOWC for Hybrid WDM-MDM Signals

The AOWC chip has exhibited the performance of large bandwidth and low crosstalk, which makes it possible to realize the AOWC scheme for hybrid WDM-MDM signals. The experimental setup is shown in Fig. 6(a). In this case, more optical carriers should be provided to support more wavelength channels. The signal channels *S*1 and *S*2 are provided by two channels of the tunable laser (see the dashed box in Fig. 6(a)) and 2 × 2 channel hybrid WDM-MDM signals are used. The wavelengths of the pump *P* and the two signals are set at 1549.3, 1550.9, and 1551.7 nm, and the corresponding powers before the waveguide are around 23.5, 20.2 and 19.9 dBm, respectively. A 10 Gbit/s OOK sequence is simultaneously modulated on signal *S*1 and signal *S*2. ODLs are introduced to eliminate the correlation of different channels. Fig. 10 presents the measured BERs and eye diagrams of the hybrid WDM-MDM signals and the converted idlers, in the case of the pump and two signals input from CH1 and CH2 input ports simultaneously. The insets of Fig. 10 show the corresponding optical spectrums measured at the output ports of the AOWC chip. The power penalties (at BER of 10^{-9}) of about 2.5 dB are obtained for the TE_0 mode idlers *I*1 (1547.7 nm) and *I*2 (1546.9 nm). The extra power penalties of 0.2 dB are obtained for the TE_1 mode idlers. Consequently, although the wavelength channels are increased from one to two channels in comparison with MDM signals, the quality of signals on the converted idlers is almost the same. This characteristic is consistent with the simulated flat conversion efficiency curve in the C-band. The clear eye-diagrams are observed in Fig. 10(b), which means that both the wavelength-converted signals are of high quality without obvious degradation compared to the input signals. Therefore, the multimode device we designed is appropriate to be applied for multi-channel AOWC of hybrid multiplexing signals.

VI. Conclusion

The FWM-based broadband AOWC scheme of hybrid multiplexing signals has been presented and experimentally demonstrated on a silicon chip, which includes a parallel dispersion-engineered multimode nonlinear waveguide with mode (de)multiplexers. The fabricated chip exhibits a coupling loss of 7.4 dB/facet, and a transmission loss of 1.2 dB/cm (or 3.0 dB/cm) for TE_0 (or TE_1) mode. In the nonlinear waveguide, the AOWC function is supported by the intra-modal FWM processes of TE_0 and TE_1 modes, and the intermodal FWM processes serve as the crosstalk. The dual-mode pump and signal are injected into the chip via an OFA. By comparing the quality of the converted signals in different wavelength channels, the effect of the intermodal crosstalk introduced by FWM processes on conversion bandwidth is discussed. The intermodal crosstalk is measured to be −25.9 dB for TE_0 (or −23.6 dB for TE_1) mode, and the conversion efficiency is −25.4 dB (or −26.3 dB) correspondingly. The crosstalk will be strengthened as the signal moves towards the pump and a 2-nm-wavelength range is not available due to the heavy crosstalk. The conversion bandwidth of MDM signal is finally evaluated to be ∼68 nm, excluding the 2 nm wavelength range near the pump. For 4 × 10 Gbit/s OOK hybrid WDM-MDM signals, the received power penalties of all the four converted channels are less than 2.7 dB at the BER of 1×10^{-9}. The proposed approach provides a new pathway for the AOWC of more-dimensional hybrid multiplexing signals, which is of great significance for the development of modern high-speed and high-capacity communication networks.

References

[1] C. A. Brackett, "Dense WDM networks: Principles and applications," *IEEE J. Sel. Areas Commun.*, vol. 8, no. 6, pp. 948–964, Aug. 1990.
[2] S. J. B. Yoo, "Wavelength conversion technologies for WDM network applications," *J. Lightw. Technol.*, vol. 14, no. 6, pp. 955–965, Jun. 1996.
[3] D. Dai and J. E. Bowers, "Silicon-based on-chip multiplexing technologies and devices for peta-bit optical interconnects," *Nanophotonics*, vol. 3, no. 4-5, pp. 283–311, Aug. 2014.
[4] N. Hanzawa et al., "Mode multi/demultiplexing with parallel waveguide for mode division multiplexed transmission," *Opt. Exp.*, vol. 22, no. 24, pp. 29321–29330, Dec. 2014.

[5] X. Zhang, M. Karlsson, P. A. Andrekson, and E. Kolltveit, "Polarization-division multiplexed solitons in optical fibers with polarization-mode dispersion," *IEEE Photon. Technol. Lett.*, vol. 10, no. 12, pp. 1742–1744, Dec. 1998.

[6] D. Dai et al., "10-channel mode (de)multiplexer with dual polarizations," *Laser Photon. Rev.*, vol. 12, no. 1, Jan. 2018, Art. no. 1700109.

[7] W. Jiang, J. Miao, and T. Li, "Compact silicon 10-mode multi/demultiplexer for hybrid mode- and polarisation-division multiplexing system," *Sci. Rep.*, vol. 9, no. 1, Sep. 2019, Art. no. 13223.

[8] L. W. Luo et al., "WDM-compatible mode-division multiplexing on a silicon chip," *Nature Commun.*, vol. 5, no. 1, Jan. 2014, Art. no. 3069.

[9] D. Dai, J. Wang, S. Chen, S. Wang, and S. He, "Monolithically integrated 64-channel silicon hybrid demultiplexer enabling simultaneous wavelength- and mode-division-multiplexing," *Laser Photon. Rev.*, vol. 9, no. 3, pp. 339–344, May 2015.

[10] C. Li et al., "Hybrid WDM-MDM transmitter with an integrated Si modulator array and a micro-resonator comb source," *Opt. Exp.*, vol. 29, no. 24, pp. 39847–39858, Nov. 2021.

[11] S. Chen, Y. Shi, S. He, and D. Dai, "Compact monolithically-integrated hybrid (de)multiplexer based on silicon-on-insulator nanowires for PDM-WDM systems," *Opt. Exp.*, vol. 23, no. 10, pp. 12840–12849, May 2015.

[12] Y. Tan, H. Wu, and D. Dai, "Silicon-based hybrid (de)multiplexer for wavelength-/polarization-division-multiplexing," *J. Lightw. Technol.,* vol. 36, no. 11, pp. 2051–2058, Jun. 2018.

[13] F. Parmigiani, Y. Jung, L. Gruner-Nielsen, T. Geisler, P. Petropoulos, and D. J. Richardson, "Elliptical core few mode fibers for multiple-input multiple output-free space division multiplexing transmission," *IEEE Photon. Technol. Lett.*, vol. 29, no. 21, pp. 1764–1767, Nov. 2017.

[14] S. Chang et al., "Mode- and wavelength-division multiplexed transmission using all-fiber mode multiplexer based on mode selective couplers," *Opt. Exp.*, vol. 23, no. 6, pp. 7164–7172, Mar. 2015.

[15] Y. Tan, H. Wu, S. Wang, C. Li, and D. Dai, "Silicon-based hybrid demultiplexer for wavelength- and mode-division multiplexing," *Opt. Lett.*, vol. 43, no. 9, pp. 1962–1965, May 2018.

[16] J. Gong et al., "All-optical wavelength conversion for mode division multiplexed superchannels," *Opt. Exp.*, vol. 24, no. 8, pp. 8926–8939, Apr. 2016.

[17] Y. Qiu et al., "Mode-selective wavelength conversion of OFDM-QPSK signals in a multimode silicon waveguide," *Opt. Exp.*, vol. 25, no. 4, pp. 4493–4499, Feb. 2017.

[18] M. Ma and L. R. Chen, "On-chip silicon mode-selective broadband wavelength conversion based on cross-phase modualtion," in *Proc. Conf. Lasers Electro-Opt.*, 2016, Paper STh3E.3.

[19] J. Xiong, Y. Yu, W. Yang, C. Sun, and X. Zhang, "Crosstalk suppressed high efficient mode-selective four-wave mixing through tailoring waveguide geometry," *IEEE Photon. J.*, vol. 11, no. 1, Feb. 2019, Art. no. 6600408.

[20] W. Pan, Q. Jin, X. Li, and S. Gao, "All-optical wavelength conversion for mode-division multiplexing signals using four-wave mixing in a dual-mode fiber," *J. Opt. Soc. Amer. B*, vol. 32, no. 12, pp. 2417–2424, Dec. 2015.

[21] Z. Xu, Q. Jin, Z. Tu, and S. Gao, "All-optical wavelength conversion for telecommunication mode-division multiplexing signals in integrated silicon waveguides," *Appl. Opt.*, vol. 57, no. 18, pp. 5036–5042, Jun. 2018.

[22] B. Chen, J. Chen, Y. Zhao, and S. Gao, "Silicon-based on-chip all-optical wavelength conversion for two-dimensional hybrid multiplexing signals," *J. Nonlinear Opt. Phys. Mater.*, vol. 28, no. 4, Dec. 2019, Art. no. 1950034.

[23] H. Hu et al., "Parametric amplification, wavelength conversion, and phase conjugation of a 2.048-Tbit/s WDM PDM 16-QAM signal," *J. Lightw. Technol.*, vol. 33, no. 7, pp. 1286–1291, Apr. 2015.

[24] L. Zhang, S. Jie, and J. Xiao, "Broadband and scalable silicon-based mode multiplexer using subwavelength-grating-based adiabatic coupler," *J. Nanophotonics*, vol. 15, no. 4, Dec. 2021, Art. no. 046010.